JOURNAL OF MATERIALS SCIENCE 21 (1986) 2889–2900

Influence of short-fibre reinforcement on the fracture behaviour of a bulk liquid crystal polymer

H. VOSS,* K. FRIEDRICH
Polymer and Composites Group, Technical University Hamburg-Harburg, 2100 Hamburg-Harburg 90, West Germany

The microstructure and some mechanical properties of a liquid crystal polymer (LCP) and its short-fibre composites have been investigated. Injection moulded plates of the latter materials exhibit a layered structure well-known for many short-fibre reinforced polymer systems. A pronounced layered structure is also found in the neat LCP matrix, superimposed by a certain degree of molecular orientation. The special, microstructural character of the matrix polymer results in a high anisotropy of the mechanical properties of all materials investigated. In particular, this is found for the tensile strength, the fracture toughness and the fatigue crack propagation. The composites show nearly no improvement or even a reduction in their performance, compared to the matrix material, as far as these properties are concerned. This can, in part, be correlated to microscopic failure mechanisms detected by scanning electron microscopy of the fractured surfaces, revealing that the fibre–matrix bond strength is relatively poor.

1. Introduction

Thermotropic liquid crystal polymers (LCP) are a relatively new class of polymers which combine the advantage of easy processability by methods common for thermoplastic polymers with outstanding mechanical properties. The material tested in this work is a wholly aromatic copolyester. Owing to the high content of aromatic units the polymer chains are relatively stiff, and the formation of a liquid crystalline mesophase is observed in the molten state [1]. Investigations of injection moulded parts of these class of polymers have been reported in the literature over the last 10 years [2]. The elongation flow fields imposed on the melt during the mould filling process give rise to a certain molecular orientation of the polymer which is maintained also in the solid material [3]. This molecular orientation, in turn, is reflected in the anisotropic mechanical behaviour of the material, with the highest values of strength and elastic modulus parallel to the flow direction [4].

As with the other thermoplastics it is possible to incorporate short fibres in the polymer matrix, in order to influence the mechanical properties of the material. It was the objective of the present study to investigate the influence of fibre reinforcement in strength and fracture mechanical behaviour of LCP. In particular, it was of special interest how the microstructural parameters such as fibre material and orientation, fibre–matrix bond quality and fibre length, influence the materials fracture toughness and resistance against fatigue crack propagation [5].

2. Experimental details

2.1. Materials

The polymer investigated in the present study is a thermotropic copolyester produced by Celanese Corporation, Summit, New Jersey 07901, USA (material code LCP, mol. wt > 20 000, T_M = 280° C). In addition to the neat polymer, four composites containing different amounts of short glass- and carbon-fibres and a mineral filler were tested. Table I lists the exact compositions and material codes. All materials had been delivered by the manufacturer as injection-moulded, end-gated, rectangular plates (Fig. 1).

2.2. Microscopy

Most of the microscopic work was done with a scanning electron microscope (SEM). Specimens used to determine the orientation distribution of the short fibres were polished with alumina and diamond powder (0.1 μm). Prior to SEM studies, these specimens, as well as those used for the fractographic analysis, were gold coated within a sputtering chamber. Thin sections taken from the neat polymeric material were examined by transmitted light microscopy. In addition, some ultra-thin sections prepared from the matrix by use of an ultrafreezing-microtome were viewed in a transmission electron microscope (TEM).

2.3. Mechanical testing

2.3.1. Tensile tests

Tensile tests were performed on a static testing machine

* *Present address*: Centre for Composite Materials, University of Delaware, Newark, Delaware 19716, USA.

0022–2461/86 $03.00 + .12 © *1986 Chapman and Hall Ltd.*

TABLE I Material codes and compositions of the LCP materials tested

	Material code				
	LCP	LCP-30 GF	LCP-50 GF	LCP-30 CF	LCP-MGF
Kind of Reinforcement	–	Glass fibres	Glass fibres	Carbon fibres	Glass fibres, mineral filler, graphite flake,
Amount of reinforcement					
(wt %)	–	30	50	30	25, 25, 5
(vol %)	–	19	35	23	18, 17, 4
Density ($g\,cm^{-3}$)	1.4	1.61	1.79	1.49	1.89

at room temperature and a cross-head speed of 50 mm min^{-1}. In order to get an idea about the mechanical anisotropy of the materials, tensile bars were machined from the plates under two different orientations, (parallel and perpendicular to the mould fill direction, MFD). Their geometry is shown in Fig. 2.

2.3.2. Fracture toughness measurements

The fracture toughness of the materials was measured by the use of compact tension (CT) specimens (Fig. 3). Their initial notch ran either perpendicular or parallel to the MFD. These different directions of crack propagation relative to MFD are referred to as transverse (T) direction and longitudinal (L) direction in the following text. Starter crack formation was carried out by driving a razor blade into the material. The following K_c measurements began with these cracks and/or with natural cracks, created by previous fatigue or K_c testing. The tests were performed on a static testing machine under stroke control, with a cross-head speed of 0.5 mm min^{-1}. Load–displacement curves were recorded on an x–y recorder. A detailed decription of the testing procedure can be found elsewhere [6].

2.3.3. Fatigue crack growth measurements

The fatigue loading was performed with the same shape of CT specimens as indicated in Fig. 3, under uniaxial tension–tension and a minimum/maximum load ratio of $R = 0.2$. The load against time function was sinusoidal with a frequency of $f = 5$ Hz. Measurements of the actual crack length were followed stepwise by the use of an optical microscope after certain numbers of loading cycles N.

3. Results and discussion

3.1. Microstructure of injection-moulded plates

3.1.1. Unreinforced LCP samples

Different microscopical methods were applied in order to investigate the microstructure of the LCP. Transmitted light micrographs are depicted in Fig. 4. The different positions, relative to the mould fill direction (MFD) from which the thin sections were taken are indicated in Fig. 4a. Fig. 4c clearly demonstrates, in agreement with previous reports [7–9], that the plate thickness, B, is built up of approximately three different layers, two surface layers (S) and a central layer (C). Flow lines are visible in the central layer. Fig. 4b reveals, that the surface layer itself consists of a set of different microlayers [9]. These observations are supported by investigations made with transmitted electron microscopy (Fig. 5). The microstructure of the material is further illustrated by scanning electron micrographs taken from an L-cracked CT-fracture surface of the neat matrix polymer.

The two surface layers and the central layer are clearly distinguishable in the overview (Fig. 6a). The flow lines in the centre region are obvious (arrow), even gaps along those lines seem to exist. Pictures taken at higher magnifications further support the results described above. Again a material behaviour which is highly fibrillar in nature is dominant in the surface regions and, on the other hand, plate-like structures appear in the central region. There is a relatively sharp transition from surface to centre layers.

A schematic sketch of the microstructure of the injection-moulded plates is given in Fig. 7. Three layers, each with a thickness of about one-third of the plates thickness, built up the material. The microlayers in the surface regions have a thickness between 0.5 and 1 μm (Fig. 6d), which is in good agreement with the dimensions of the microlayers found by Weng *et al.* [9]. The results of the TEM work show that the dimensions of the single fibrils are at about 0.02 μm. The plate like structures in the central layer are about 5 μm in lateral size and 2 to 3 μm in thickness. But the TEM-micrographs also reveal fine structures of about 0.2 μm.

3.1.2. Composites

The short-fibres in the reinforced materials exhibit an orientation distribution well-known for injection

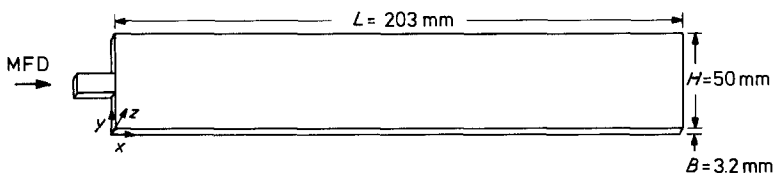

Figure 1 Geometry of the injection-moulded plates, with the mould fill direction (MFD) indicated.

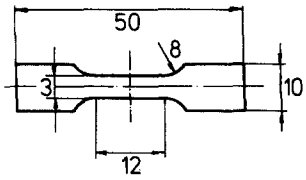

Figure 2 Geometry of the tensile bars used for the tensile tests (mm).

moulded short-fibre reinforced thermoplastics [10]. SEM micrographs taken from polished surfaces of glass fibre composites are given in Fig. 8. There are three different layers distinguishable. The fibres have a preferred orientation which is parallel to the MFD in the two surface layers and perpendicular to the MFD in the central layer (Fig. 8a). The degree of orientation increses with increasing amounts of reinforcement (Figs 8b and c) and can be quantified by a fibre orientation parameter f_p

$$f_p = 2\langle\cos^2\theta\rangle - 1 \qquad (1)$$

where θ is the angle between a single fibre and the MFD. A somewhat different microstructure is observed in the case of carbon-fibre reinforcement. Two additional regions just below the surface of the plates appear in this case, with a nearly random orientation of the short fibres (Regions S in Fig. 9a). The layers with a high degree of orientation in MFD are below these layers (I) and are reduced in thickness, compared to the other composites. An exception is found for the mineral filled composite, in which the orientation parameter is relatively low (Fig. 9b). The size of the mineral filler particles varies between 10 and 150 μm. Most of the microstructural parameters evaluated for the different materials are summarized in Table II.

One additional microstructural parameter which is also of some importance, is the length distribution of the short-fibres. In order to get some information about fibre length, small samples were cut and the matrix was burned off. The remaining fibres were viewed in a light microscope so that the fibre length could be determined. The fibre length distribution of

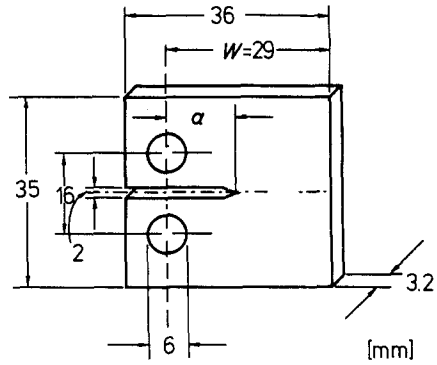

Figure 3 Geometry of compact tension (CT) specimens used for K_c testing and fatigue crack propagation.

the glass-fibre composites is given in Fig. 10. It is obvious that the average fibre length is reduced the more fibres are added. This reduction is probably due to enhanced fibre breakage events during the mould filling process of specimens with higher fibre content. The average values of fibre length in the different composites are: LCP-30 GF: $\bar{l} = 160\,\mu$m; LCP-50 GF: $\bar{l} = 130\,\mu$m; LCP-30 CF: $\bar{l} = 180\,\mu$m; LCP-MGF: $\bar{l} = 100\,\mu$m.

3.2. Mechanical test results

3.2.1. Tensile tests

Results of the tensile tests obtained with the neat LCP and the glass-fibre composites are given in Fig. 11. The high anisotropy in mechanical behaviour is clearly reflected in a reduction of tensile strength by a factor of about 2 if the cracks propagate parallel to MFD (L-crack-direction; with load perpendicular to MFD). This anisotropy seems to be due mainly to the molecular orientation of the polymer and not to the orientation of the glass-fibres in the composites, because there is no difference in the degree of anisotropy found between the neat polymer and its fibre composites. The tensile strength is not improved by adding fibres, there is even a considerable reduction for the higher fibre loadings. These results are in some contrast to data supplied by the manufacturer, in

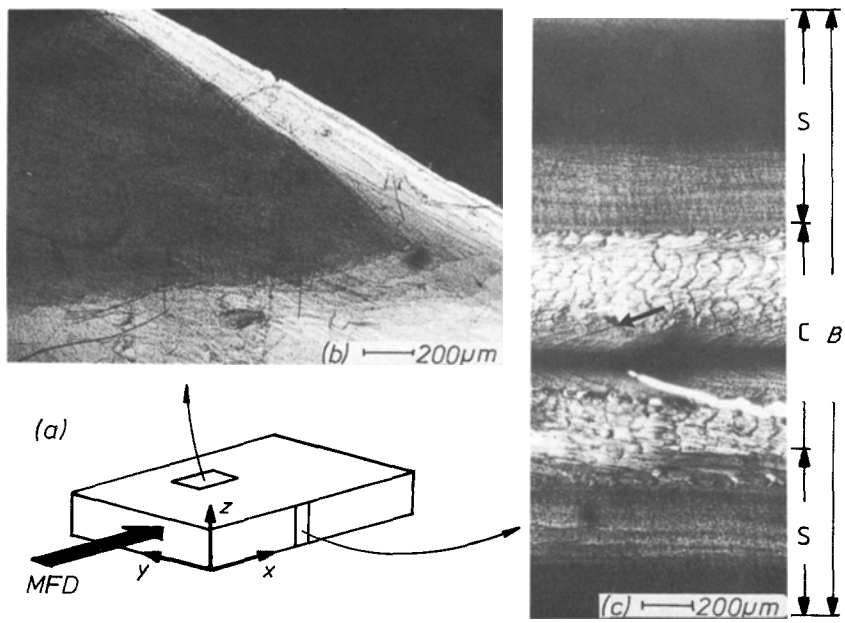

Figure 4 Transmitted light micrographs from thin cuts taken at different locations as indicated in (a), parallel to the plate's surface (b) and across the plate's thickness (c). Fig. (b) shows that the polymer consists of microlayers and is fibrillar in nature in the surface regions. Micrograph (c) shows the microlayers, i.e. two surface layers S and a central layer C with conical flow lines in it (arrow).

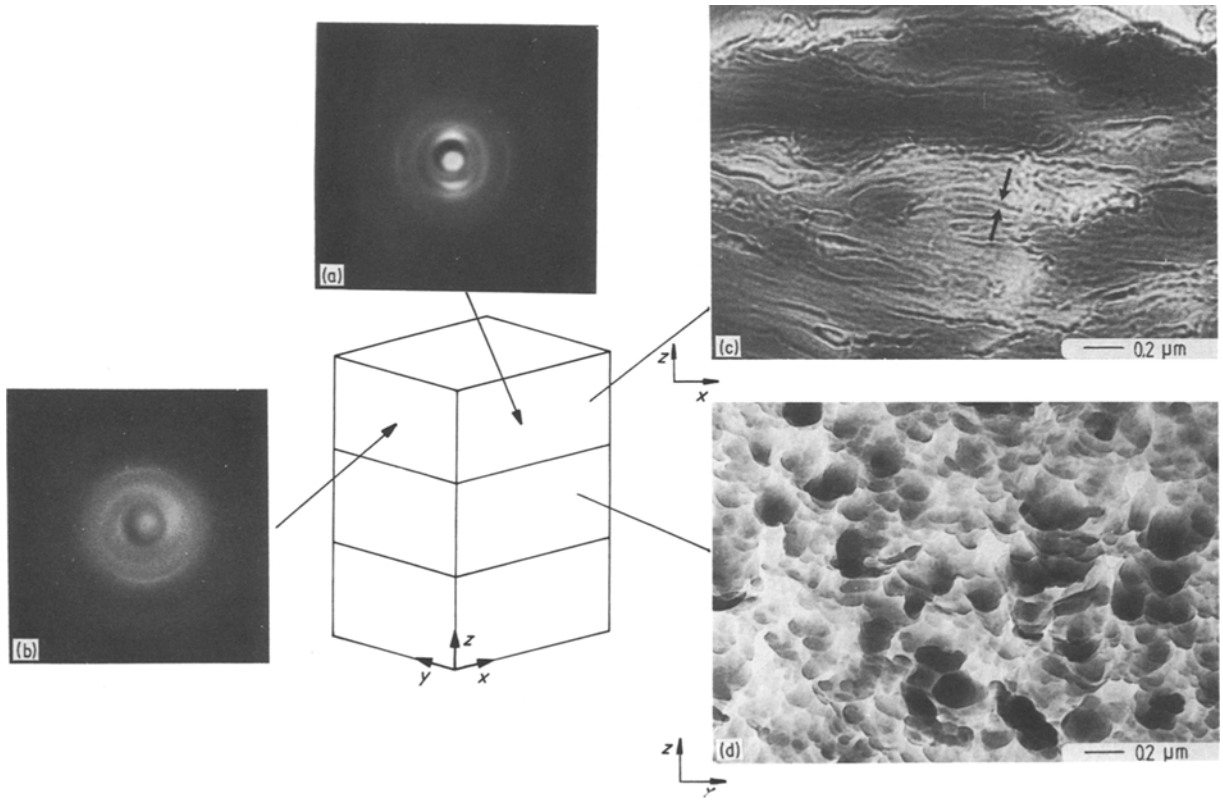

Figure 5 Transmitted electron micrographs, (a) showing a diffraction pattern with the incident beam parallel to the y-axis, i.e. perpendicular to the MFD, the orientation parallel to the MFD is visible. An electron diffraction pattern parallel to MFD is depicted in (b). No orientation is visible here. The bright-field image (c) depicts the fibrillar structure of the surface region, a single fibril is marked by the arrows, with a thickness, t_f, of about 0.02 μm. (d) Shows the domain-like nature of the centre layer.

particular the results obtained here for the material with 35 vol % GF reveal a much lower value. These deviations may, in part, reflect that our samples were machined from rectangular plates whereas the manufacturer had used injection-moulded tensile bars.

3.2.2. Fracture toughness studies

Fracture toughness measurements were performed with CT-specimens which were notched in L- and T-direction, as mentioned above. The load at which unstable crack growth occurred in the case of T-cracks by far exceeds the corresponding level for L-cracks. But the T-cracks do not propagate in a plane perpendicular to the load direction, so that it is not possible to derive valid K_{Ic} values from these tests. Two load–displacement curves of L-cracked samples of the matrix material and the material reinforced with 35 vol % glass fibres are compared in Fig. 12. The matrix material shows a very ductile behaviour whereas the composite fails in an almost brittle manner. This different behaviour is displayed in the relative values of the load maximum F_{max} and a load F_q, where F_q is the value at the intercept with a straight line which has a slope of 95% of the linear part of the load displacement curve [11]. These values are nearly identical with F_{max} for the composite material, in contrast to the matrix material where a big difference between the two load levels exists. If K_c values are calculated according to the following equation:

$$K_c = \frac{F_c}{BW^{1/2}} Y(a/W) \tag{2}$$

where

$$Y(a/W) = 29.6(a/W)^{1/2} - 185.5(a/W)^{3/2} + 655.7(a/W)^{5/2} - 1017(a/W)^{7/2} + 638.9(a/W)^{9/2} \tag{3}$$

(a is the crack length, B the specimen thickness and W the specimen width) one comes up with the results given in Fig. 13. The data were calculated for $F_c = F_q$, which gives a more realistic picture of the material behaviour in terms of a fracture mechanical approach. Only for comparison, the $K_{c_{max}}$ value of the matrix material is also included. It indicates that in this case the transition from stable (K_{c_q}) to unstable

TABLE II Microstructural parameters of the composite materials. C/B is the ratio of central layer thickness to plate thickness, $f_{p(c)}$ the fibre orientation parameter in the central layer, relative to MFD. $2S/B$ is the ratio of the surface layers to the plate thickness and $f_{p(s)}$ the fibre orientation parameter in these layers. The surface layers are subdivided into two layers in the case of the carbon-fibre reinforced composite (Fig. 9a)

Composition	C/B	$f_{p(c)}$	$2S/B$			$f_{p(s)}$
19 vol %	0.3	0.6	0.7			−0.6
35 vol %	0.3	0.8	0.7			−0.8
18 vol % GF + min fill	0.25	0.2	0.75			−0.2
			S_s	S_I	S_s	S_I
23 vol % CF	0.4	0.85	0.24	0.36	0	−0.85

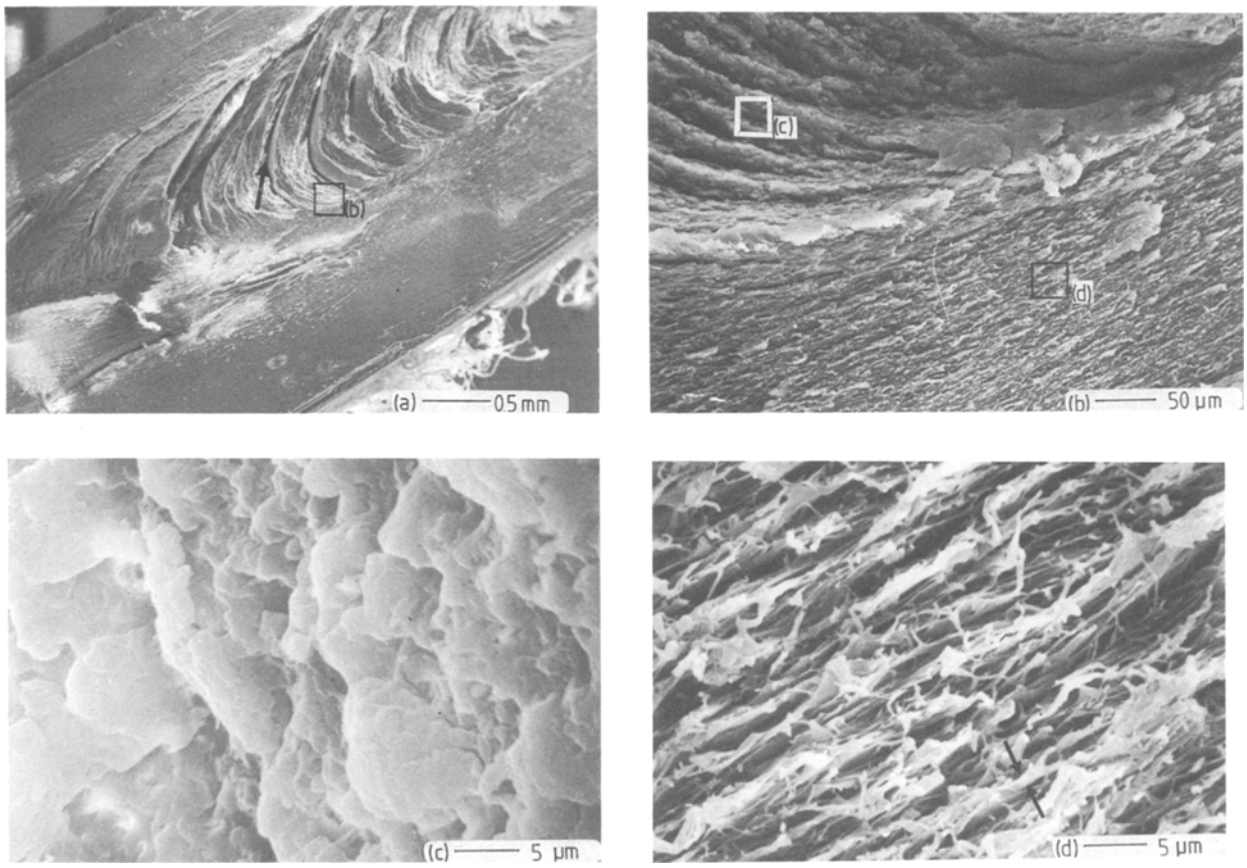

Figure 6 Scanning electron micrographs of a fracture surface after fatigue crack propagation in L direction. The direction of crack growth is from lower left to upper right corner in all micrographs. (a) An overview of the fracture surface, the three different layers are clearly distinguishable, a flow line with a small gap along it is marked by an arrow. The transitional region of surface layer to central layer is shown in (b), at higher magnification, taken at the position indicated in (a). The boundary between the two layers is very sharp. (c) and (d) High magnifications of parts of the central and surface layer, respectively, indicated in (b). The plate-like domains in (c) have a thickness t_d of about 2 to 3 μm and a diameter d_D of about 5 μm. The microlayers, which build up the surface layers, appear in (d), having a thickness t_{ML} of 0.5 to 1 μm.

crack propagation ($K_{c_{max}}$) requires an additional high amount of fracture energy.

The course of the K_c values plotted against volume fraction of reinforcement (Fig. 13) is very similar to the behaviour of the tensile strength, again no improvement is achieved by adding reinforcements to the matrix (with the exception of short-carbon fibres). This is often found for matrices which behave very ductily [5].

3.2.3. Fatigue crack propagation

In addition to the static fracture tests, the resistance of the materials against fatigue crack propagation was investigated. Values of the propagation rate, da/dN, were determined from the slope of the crack-length against loading cycle curves. The corresponding stress intensity factor range ΔK_I was calculated by

$$\Delta K_I = \frac{\Delta F}{BW^{1/2}} Y(a/W) \tag{4}$$

It is well known, that the fatigue crack propagation behaviour of many materials, among which are many polymers, follows an empirical relationship known as Paris law:

$$\frac{da}{dN} = A(\Delta K_I)^n \tag{5}$$

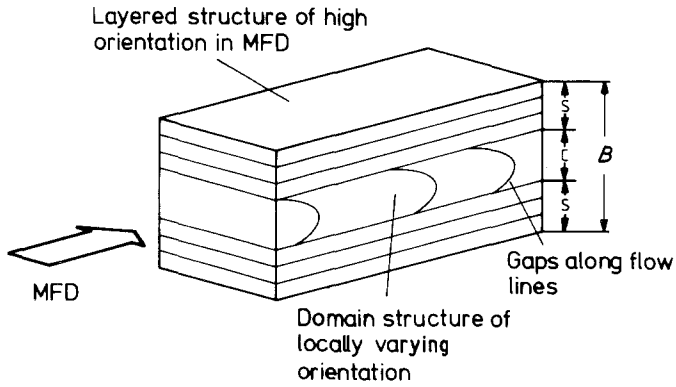

Figure 7 Schematic sketch of the microstructure of injection moulded plates. The plates consist of two surface layers, S, and a central layer, C, each of these layers is subdivided into smaller microstructural elements.

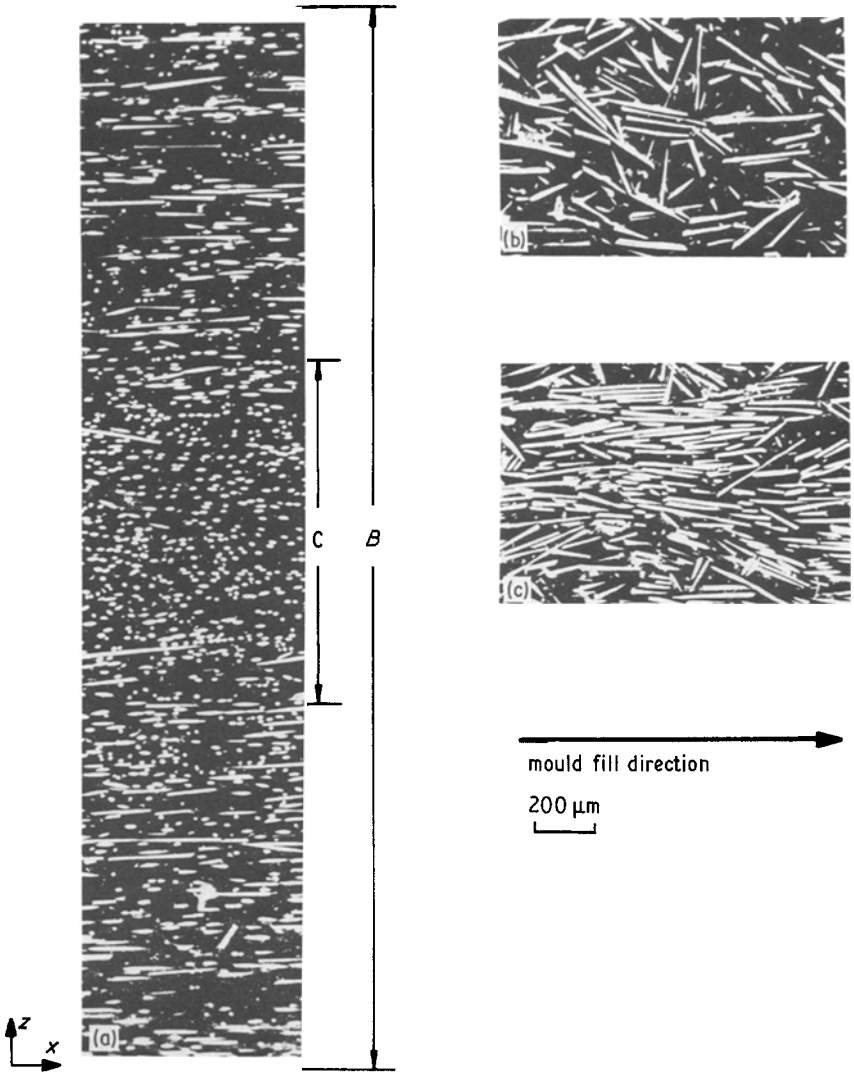

Figure 8 Scanning electron micrographs of polished surfaces of glass-fibre reinforced LCP. The layered structure across plate thickness is obvious in micrograph (a) for LCP-30 GF. The degree of fibre alignment parallel to the MFD is visible in (b) for LCP-30 GF and in (c) for LCP-50 GF. The high orientation in the latter is obvious.

Plotting log da/dN against log ΔK_I for all the materials investigated here, one finds a quite good fit to this relationship, in the range of stress intensity levels used (Figs 14 and 15).

Again, only cracks propagating in L-direction could be investigated because T-cracks did not propagate in a plane perpendicular to the load direction. The exponent n lies between 12 and 15 with the exception of the mineral filled material, where n is 8.4. The results of the fatigue crack propagation of the neat LCP and the two glass-fibre reinforced materials are in good agreement with the fracture toughness data, i.e. the da/dN curve of a material with a higher K_c value is shifted to higher ΔK_I values.

The situation is more complex in the case of LCP-30 CF and LCP-MGF. The carbon-fibre reinforced LCP and the two glass-fibre reinforced materials are its K_c value is concerned, but its da/dN curve lies between the curves of the matrix and the 19 vol % glass-fibre material. The value of K_{Ic} reflects changes in both G_{Ic} and E:

$$K_{Ic} = (G_{Ic}E)^{1/2} \qquad (6)$$

where E is the elastic modulus. On the other hand, fatigue crack propagation is more influenced by the energy absorbing mechanisms of the materials. These do not seem to depend much on the kind of fibres in this case (see the fractographic analysis below).

Thus the different trend in K_c value and da/dN curve may display the difference in modulus, due to the higher stiffness of the carbon fibres. The large, weakly bonded mineral particles in LCP-MGF are expected to reduce the energy absorbing capability of this material. This seems to be mainly important at lower crack velocities, where the behaviour of this material is worst. At larger crack velocities, close to crack instability, the modulus of the material becomes effective (Equation 6) and the da/dN curve approaches the curves of the other materials.

3.3. Microscopic failure mechanisms

3.3.1. Tensile specimens

Fractured samples were examined by light microscopy and scanning electron microscopy in order to learn about the failure mechanisms. As already mentioned, the direction of crack propagation relative to MFD had a great influence on the fracture behaviour of the LCP materials. Fig. 16 gives a comparison of both L- and T-cracked tensile specimens. The different behaviour of the layers is obvious in Fig. 16b with fibrillation in the two surface layers and separation along a flow line in the centre. Fig. 17 shows a side view of a fracture surface of a tensile bar with 19 vol % GF reinforcement. The bonding at the fibre–matrix interface seems to be not very good, as can be concluded from the length of the fibres pulled out of the matrix.

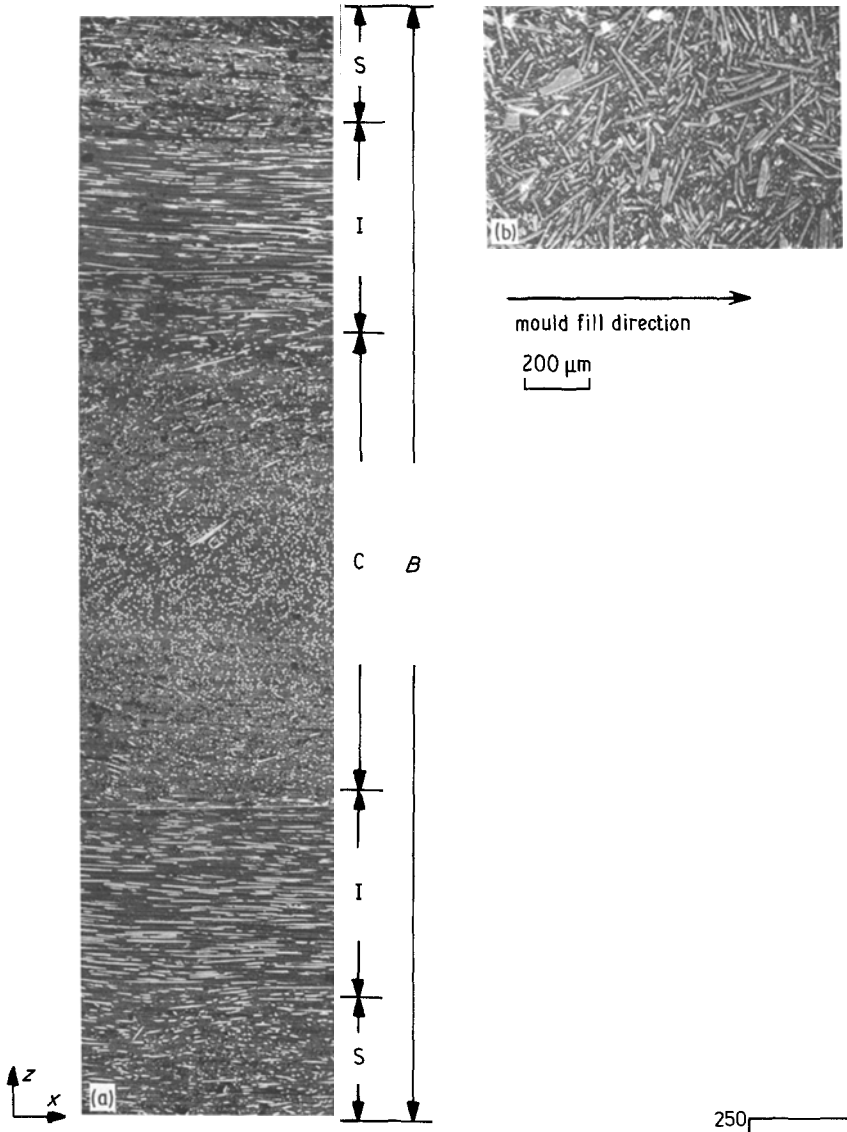

Figure 9 Scanning electron micrographs of polished surfaces of reinforced LCP. The microstructure of the LCP-30 CF is shown in (a). The carbon-fibres are randomly oriented in the layers S just below the surfaces and are oriented parallel to the MFD in the layers I and perpendicular in C. (b) Micrograph from the surface of the mineral filled LCP-MGF showing a relatively low degree of fibre orientation.

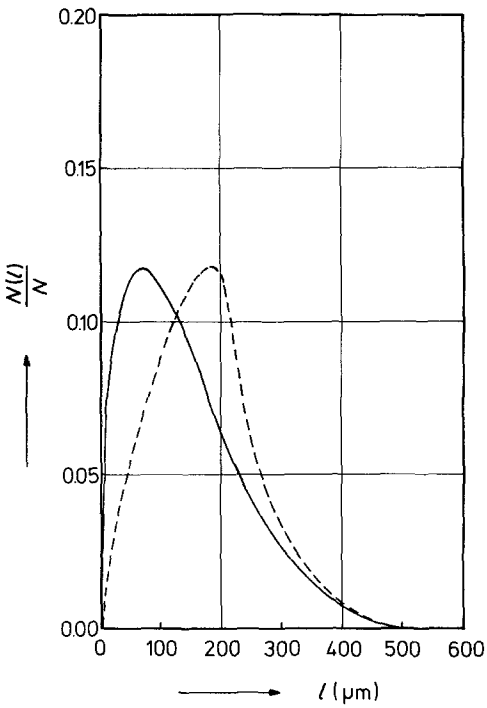

Figure 10 Length distribution of glass fibres for ---- 19 and ——— 35 vol % glass-fibre content. $N(l)/N$ is the ratio of the number of fibres of a certain length to the number of all fibres, l is the fibre length (μm).

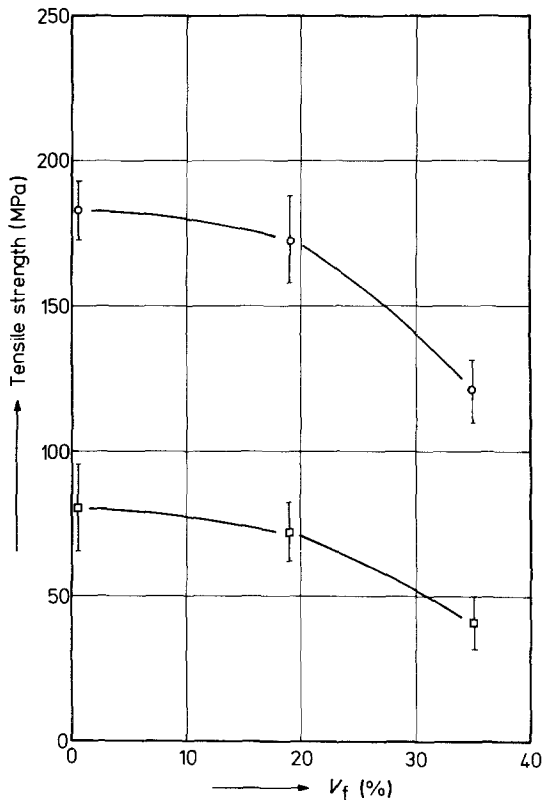

Figure 11 Tensile strength of unreinforced and glass-fibre reinforced LCP materials plotted against the volume fraction of fibres. The tensile bars were cut parallel and perpendicular to the MFD. □ L direction, ○ T direction.

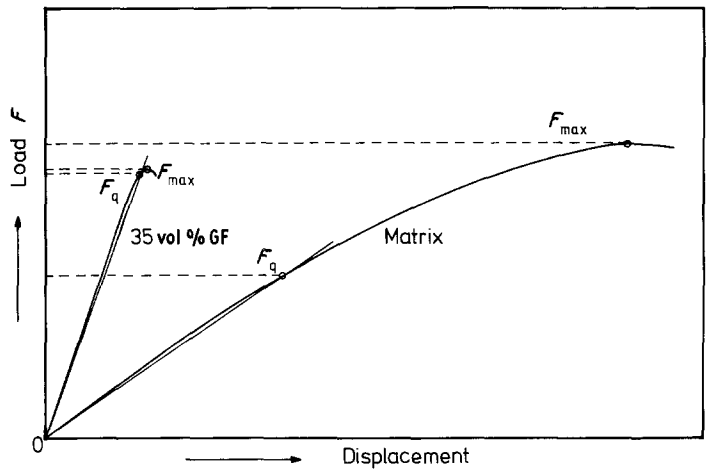

Figure 12 Schematic drawing of typical load–displacement curves derived in fracture toughness testing. F_{max} is the maximum load in the cycle and F_q the load at the intercept with a straight line having a slope of 95% of the linear part of the curve. These values are nearly identical for the fibre-reinforced material and a large difference is observable for the matrix material.

There also is not much matrix material adhering to the fibres.

3.3.2. Compact tension specimens

The fracture surface of an unreinforced sample has already been presented in Fig. 6. Looking at the glass-fibre reinforced specimens the same clear difference in the fracture mode of the layers can be recognized. The crack propagates in a smooth manner in both side layers, i.e. parallel to the main fibre orientation, whereas very rough structures appear in the central layer where the crack runs perpendicular to the fibres (Fig. 18a). This is further illustrated in the micrographs taken at higher magnification (Figs 18b to d). The resistance against crack propagation is small in the side layers if compared to the central region. Here the fibres can more effectively hinder the crack to propagate. At lower crack velocities, the crack tends to avoid the fibres and propagates along fibre ends (Fig. 18c), but at higher velocities the fracture surface becomes smoother and the fibres are mainly pulled out of the matrix (Fig. 18d).

Fig. 19 shows optical micrographs of CT-specimen surfaces in which cracks have propagated in L and T directions, respectively. The T-crack changes its direction and tends to run parallel to the predominant fibre direction. This behaviour was observed for all materials tested. The overall appearance of the fracture surfaces of the carbon-fibre reinforced composites is very similar to the glass-fibre composites (Fig. 20a). Again the surface is rough in the region where the fibres are perpendicular to the crack direction (Fig. 20b) and the dominant failure mode is fibre pull-out. There seems to be no good fibre–matrix bonding at the interface, no polymeric material is adhering to the fibres (Fig. 20c).

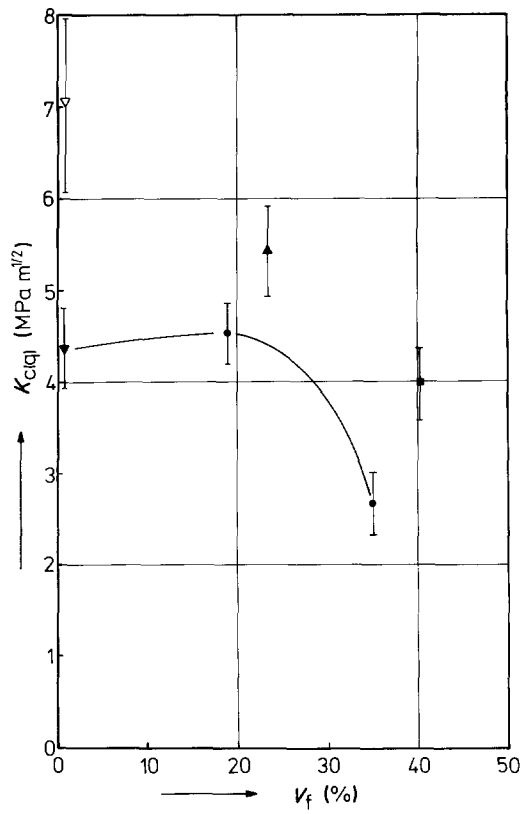

Figure 13 K_c value calculated with $F_c = F_q$, plotted against fibre volume fraction. The value calculated with $F_c = F_{max}$ is also included for the neat matrix material, being nearly twice as large as the $K_{c(q)}$ value. ▼ Matrix, ▽ $K_{c,max}$, ● glass fibre, ■ glass fibre and filler, ▲ carbon fibre.

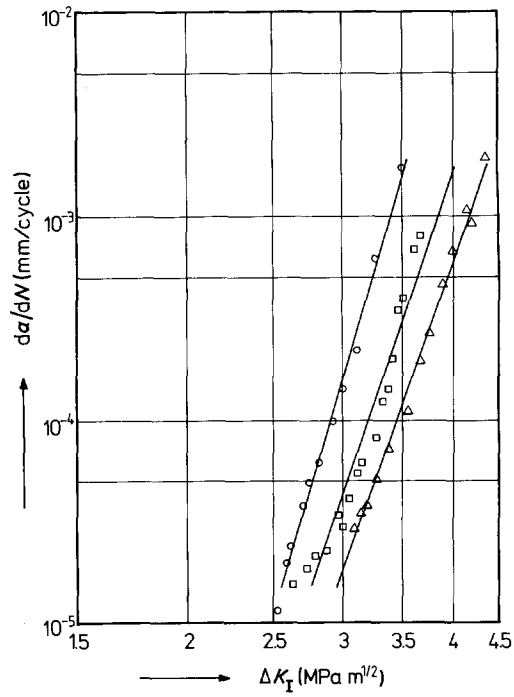

Figure 14 log da/dN against log ΔK_I curves for the neat LCP material (L direction) and two glass-fibre composites. □ Matrix, △ 19 vol % GF, ○ 35 vol % GF.

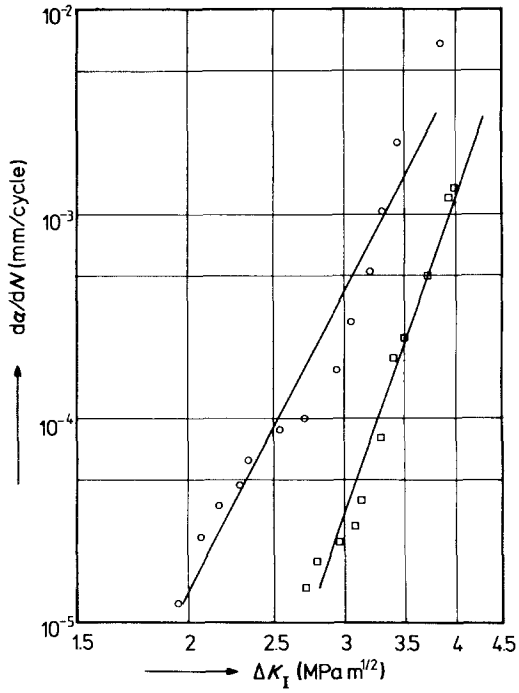

Figure 15 log da/dN against log ΔK_I curves for the carbon-fibre and glass-fibre + mineral-filled LCP composites (L direction) ○ 18 vol % GF + mineral filler, □ 23 vol % CF.

Fig. 20d shows a part of a fracture surface of a glass-fibre plus mineral-filled composite, a large filler particle is visible in the middle of the micrograph. If the crack front reaches such a particle, it is forced to change its direction and to run along the surface of this particle. This is also reflected in Fig. 21 where a polished surface of such a composite is depicted. This crack-stopping effect of the mineral filler may, in part, explain the unexpectedly high K_c value of the mineral-filled composite, compared to the composites filled with glass fibres only (Fig. 13).

3.4. Analysis of strength properties

The LCP has good mechanical properties, superior to

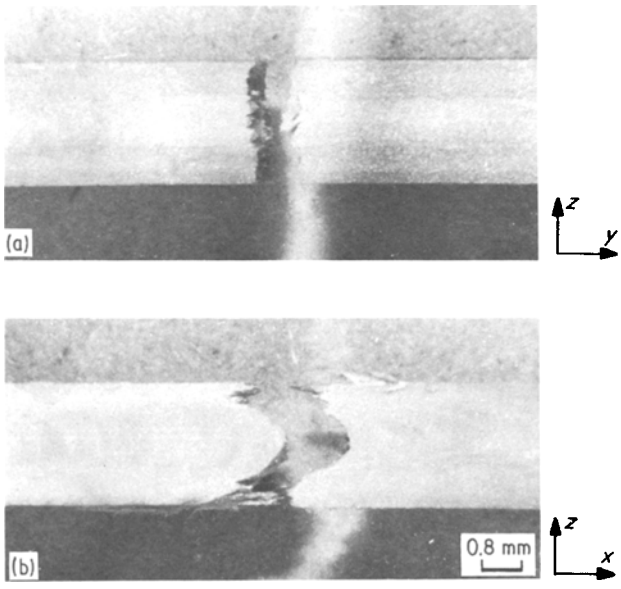

Figure 16 Fractured tensile bars of LCP-50 GF. The crack ran in the L direction in the specimen shown in (a) and the T direction in that shown in (b). The surface and central layers are distinguishable.

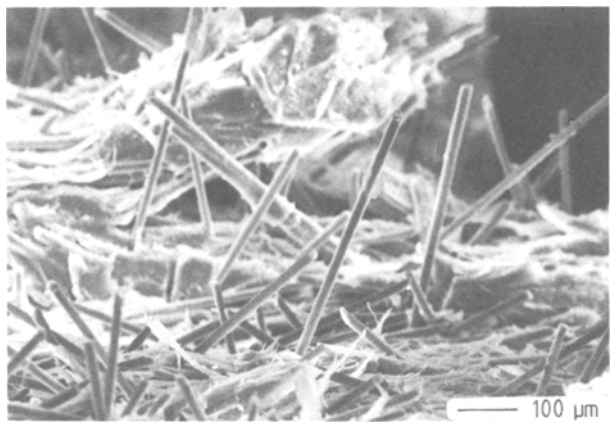

Figure 17 Scanning electron micrograph of a fracture surface of a tensile bar, viewed perpendicular to the loading direction (LCP-30 GF, L region). The long fibres pulled-out of the matrix are visible.

most of the other thermoplastic polymers. This is due to the orientation of the molecules in the liquid crystalline morphology, which is most effective if the load is applied parallel to the molecular axis and if a developing crack has to cross the orientation direction. In this case the crack tends to run parallel to the molecular axis, and crack growth in other directions is hindered.

A surprising result is that no improvement in strength and fracture toughness is achieved by adding short glass fibres to the matrix. We have applied a theoretical model in order to understand this behaviour. In a simple approach, the tensile strength of a short fibre composite can be calculated by the following rule-of-mixtures equation [12, 13]:

$$\sigma_c = \Phi\eta\sigma_f V_f + (1 - V_f)\sigma_m^* \qquad (7)$$

The first term describes the load carrying capacity of the fibres and the second the strength of the surrounding matrix.

V_f is the fibre volume fraction σ_f and σ_m^* are the strengths of the fibres and the matrix material, respectively. The factor η considers the orientation efficiency of the reinforcing fibres, ηV_f is equal to the "reinforcing effectiveness parameter" introduced by Friedrich [5] and is a function of the microstructural parameters given in Table II. Φ is the length efficiency factor, influenced both by the average fibre length, $\bar{l}$, and by the critical fibre length l_c. The latter can be estimated from the pull-out length of the fibres shown in Fig. 17. The pull-out length should not be larger than $l_c/2$ and this suggests that an l_c values of about 1000 μm is reasonable for the glass fibres. This is very large compared to l (Table II) and in this case Φ can be written as [14]:

$$\Phi = \frac{\bar{l}}{2l_c} \qquad (8)$$

The calculation was carried out separately for L and T directions using the measured matrix strengths as σ_m^*. The results are compared with the experimental values in Fig. 22 and are in good agreement for 19 vol % GF, but the calculated strength is too high for 35 vol % GF. This may be due to the fact that some mechanisms which tend to weaken the material

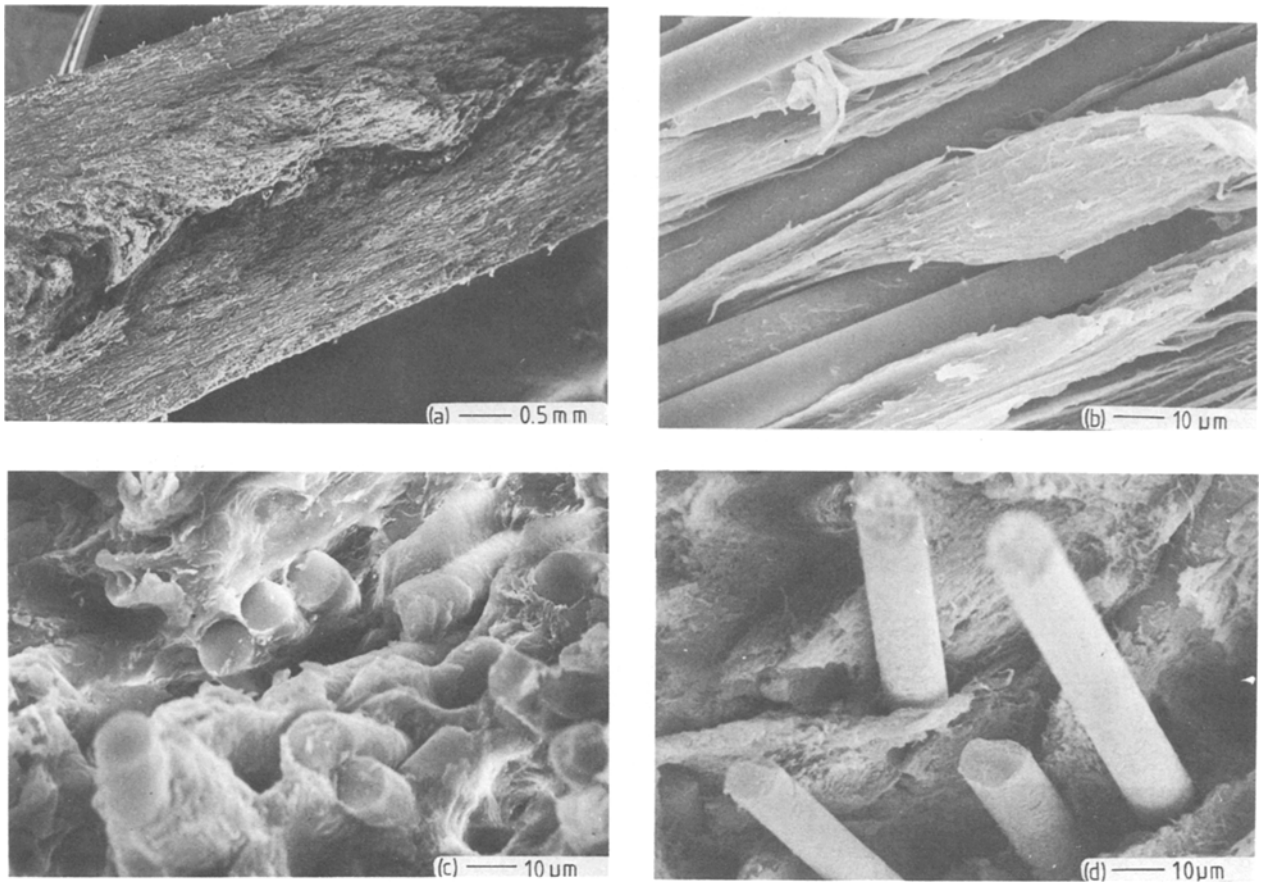

Figure 18 Scanning electron micrographs of fracture surfaces of glass-fibre LCP (L-crack). The direction of crack propagation is from lower left to upper right corner. (a) An overview; the three layers of the plate are visible. (b) High magnification micrograph out of the surface layer; the crack is running parallel to the fibres in this layer. (c) and (d) were taken at high magnifications in the central layer. The crack tends to run along fibre ends (c) at lower crack velocities and pull-out is the dominant failure mode at higher crack velocities (d).

at higher fibre loadings, such as formation of fibre bundles, were not accounted for in this approach. So one can conclude that the composites strength is not improved by the fibres because the fibre–matrix bonding is very poor. The quality of the fibre–matrix interface is expressed by the critical fibre length in our model. The same calculation carried out with $l_c = 200\,\mu m$ (Equation 8 has to be modified in this case according to [14]) demonstrates the large influence of this factor (Fig. 22). The fibre–matrix bond strength influences the K_c value in the same direction, so that both material properties could be improved by improving the bond quality.

4. Summary

It was the objective of this work to investigate the influence of short-fibre reinforcement on the fracture behaviour of a liquid crystal polymer. These properties were found to be strongly influenced by the molecular orientation and the layered structure of the polymeric matrix, leading to a high anisotropy in mechanical properties. The addition of short-fibres gives no improvement in the materials performance as far as strength and toughness are concerned. Fractographic analysis revealed that the dominating fibre related failure mechanisms are debonding at the fibre–matrix interface and fibre pull-out. These observations lead to the conclusion that poor fibre–matrix bonding is in part responsible for the composites behaviour and that it should be possible to enhance the reinforcing efficiency, in terms of strength and toughness, by further impoving the bond quality.

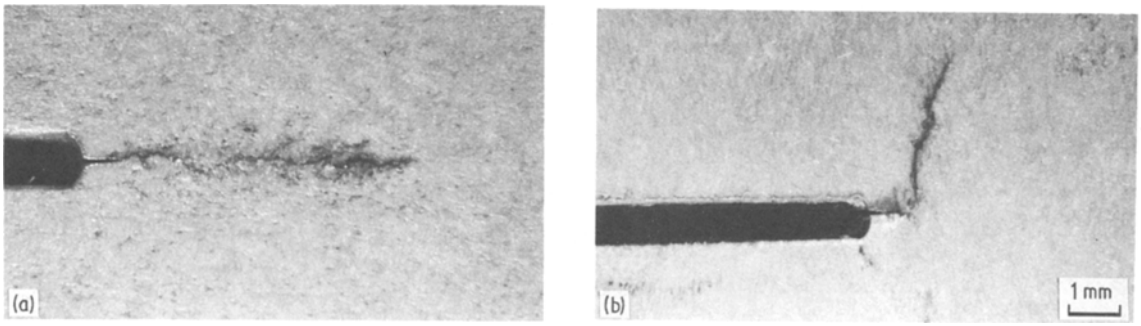

Figure 19 Optical micrographs of cracked regions of CT-specimens of LCP-30 GF after preceding fatigue crack propagation. The crack is running parallel to the MFD (L direction) in (a) and perpendicular to the MFD in (b) (T direction).

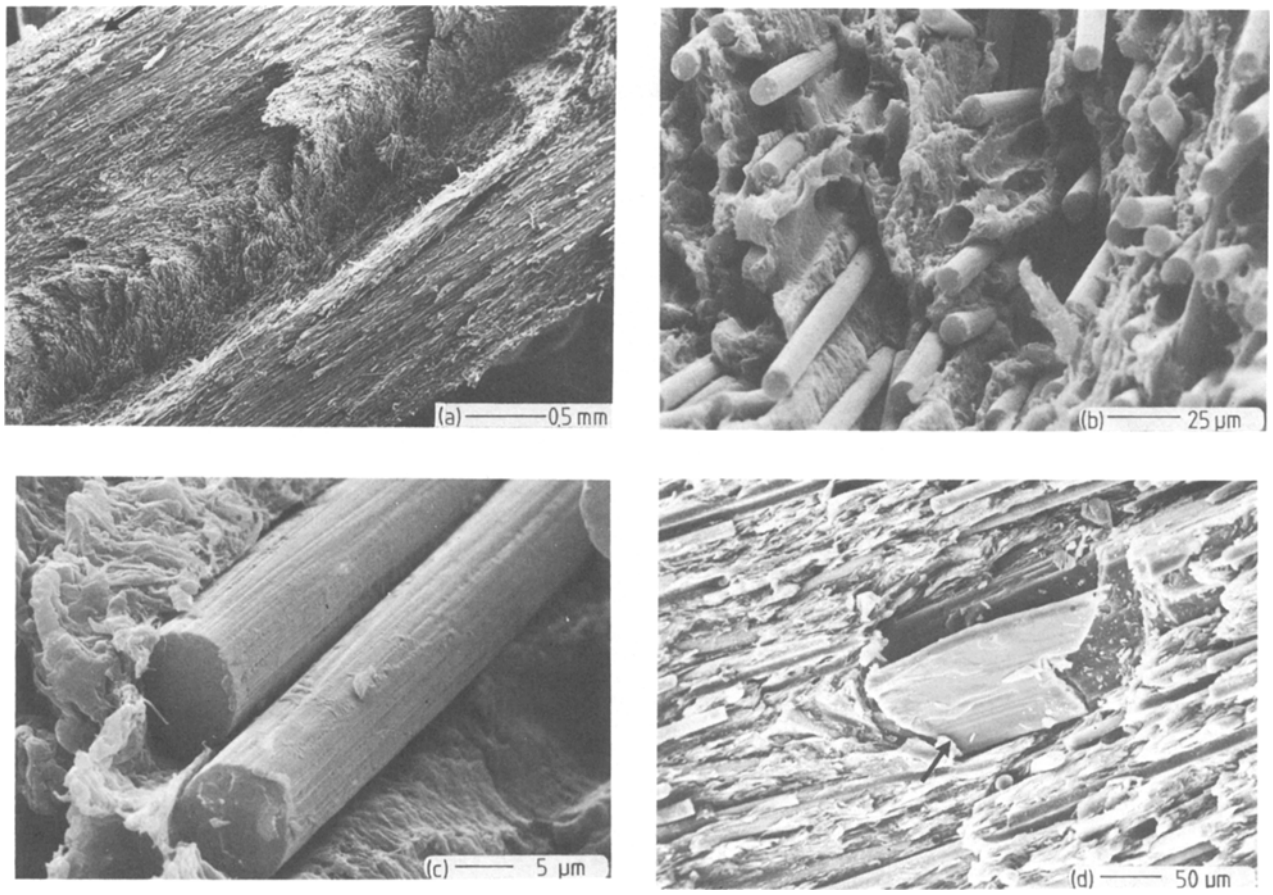

Figure 20 Scanning electron micrographs of fracture surfaces in the L direction. (a) An overview of a carbon-fibre filled composite, the different layers, including the unoriented layer at the surface (arrow), are distinguishable. (b) and (c) Details of the central layer at higher magnification. There is almost no polymeric material adhering to the carbon-fibres, so that a poor bonding of the fibres is expected. (d) Part of a fracture surface of a GF + mineral-filled composite; a large mineral particle is included (arrow), poorly bonded, with no matrix adhering. The crack is running from lower left to upper right corner in all micrographs.

Additional studies have shown that a different picture arises if the influence of fibre reinforcement on the wear behaviour of these materials is considered. This will be discussed in a second paper.

Acknowledgements
The authors gratefully acknowledge the help of Dipl.-Ing. R. Walter in performing part of the mechanical tests and of Dipl.-Ing. G. Broza in doing the transmission electron microscopy. The materials were kindly

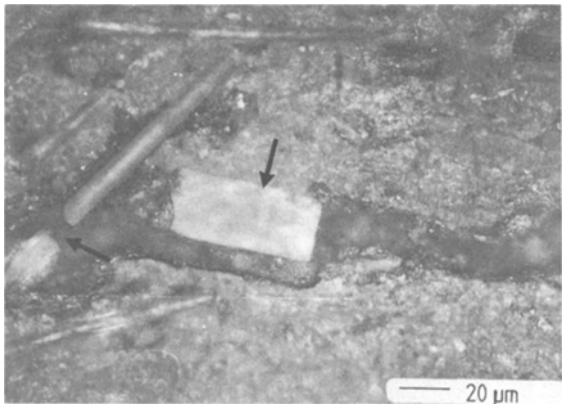

Figure 21 Polished surface of LCP-MGF with a crack which propagated from left to right. A broken glass fibre and a mineral-filler particle are visible (arrows). The crack was forced to propagate along the particle surface and had to change its direction.

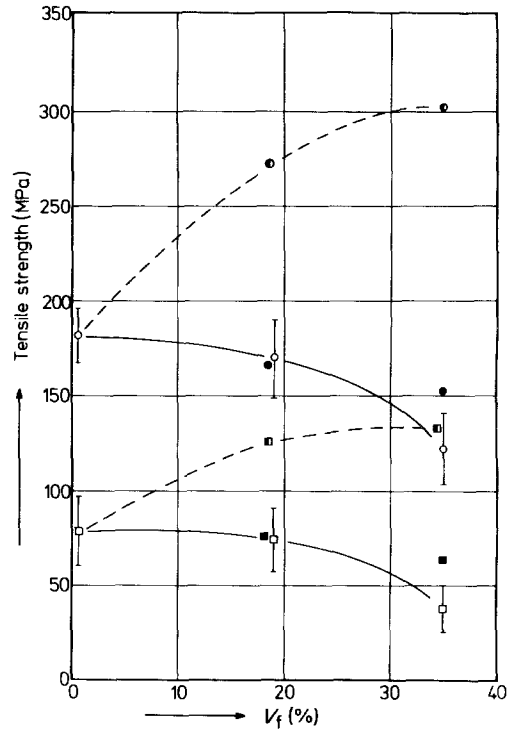

Figure 22 Comparison of experimental and calculated values of the tensile strength of glass-fibre reinforced LCP. Equation 7 was used for the calculations, with two different values for critical fibre length l_c; σ_f was taken to be 2400 MPa. The strong dependence of tensile strength on l_c, i.e. fibre–matrix bonding, is obvious. L direction: □ experimental values; calculated values, □ l_c = 1 mm, ◧ l_c = 0.2 mm. T direction; ○ experimental values; calculated values, ● l_c = 1 mm, ◐ l_c = 0.2 mm.

provided by Celanese Corporation, Summit, New Jersey, USA. The final preparation of the paper was carried out during a research stay at the Center for Composite Materials (CCM) of the Univesity of Delaware, USA. Both authors would like to thank the CCM and especially Professor R. B. Pipes (Dean of Engineering, University of Delaware) for the financial support of this endeavour.

References

1. D. J. BLUNDELL, *Polymer* **23** (1982) 359.
2. W. J. JACKSON and H. F. KUHFUSS, *J. Polym. Sci. Chem. Edn.* **14** (1976) 2043.
3. Y. IDE and Z. OPHIR, *Polym. Enging. Sci.* **23** (1983) 261.
4. M. G. DOBB and J. E. McINTRE, in "Advances in Polymer Science 60/61, Liquid Crystal Polymer II/III", edited by M. Gordon (Springer, Berlin, 1984) p. 62.
5. K. FRIEDRICH, *Composite Sci. Technol.* **22** (1985) 43.
6. *Idem, Plast. Rub. Proc. Appl.* **3** (1983) 255.
7. Z. OPHIR, Y. IDE, *Polym. Enging. Sci.* **23** (1983) 792.
8. H. TAPOR, M. BEVIS, *J. Mater. Sci. Lett.* **2**(1983) 733.
9. T. WENG, A. HILTNER, E. BAER, *J. Mater. Sci.* **21** (1986) 744.
10. K. FRIEDRICH, *Fortschr. Ber.* VDI-Z., Reihe 18, Nr 8 (1984).
11. ASTM-E399, Annual Book of ASTM Standards (American Society for Testing and Materials, Philadelphia, 1981) p. 588.
12. D. C. PHILLIPS, B. HARRIS, in "Polymer Engineering Composites", edited by M. O. W. Richardson (Applied Science, London, 1977) p. 45.
13. M. J. FOLKES, 'Short Fibre Reinforced Thermoplastics", (Wiley, Chichester, 1982).
14. J. B. SHORTALL, D. PENNINGTON, *Plast. Rub. Proc. Appl.* **2** (1982) 33.

Received 16 September
and accepted 10 October 1985